Continuous and discrete representations of feature-based attentional priority in human frontoparietal network

Mengyuan Gong & Taosheng Liu

Routledge
Taylor & Francis Group

Continuous and discrete representations of feature-based attentional priority in human frontoparietal network

Mengyuan Gong [ID] and Taosheng Liu [ID]

Department of Psychology, Michigan State University, East Lansing, MI, USA

ABSTRACT

Previous studies suggest that human frontoparietal network represents feature-based attentional priority, yet the precise nature of the priority signals remains unclear. Here, we examined whether priority signals vary continuously or discretely as a function of feature similarity. In an fMRI experiment, we presented two superimposed dot fields moving along two linear directions (leftward and rightward) while varying the angular separation between the two directions. Subjects were cued to attend to one of the two dot fields and respond to a possible speed-up in the cued direction. We used multivariate analysis to evaluate how priority representation of the attended direction changes with feature similarity. We found that in early visual areas as well as posterior intraparietal sulcus and inferior frontal junction, the patterns of neural activity became more different as the feature similarity decreased, indicating a continuous representation of the attended feature. In contrast, patterns of neural activity in anterior intraparietal sulcus and frontal eye field remained invariant to changes in feature similarity, indicating a discrete representation of the attended feature. Such distinct neural coding of attentional priority across the frontoparietal network may make complementary contributions to enable flexible attentional control.

Goal-directed attention is critical to adaptive behavior in a complex environment. It biases the neural representation among sensory stimuli (Desimone & Duncan, 1995; Kastner & Ungerleider, 2000), rendering task-relevant features or objects to attain processing priority. While much has been learned regarding the neural representation of spatial priority (Bisley & Goldberg, 2010; Ptak, 2012; Silver & Kastner, 2009), how the brain represents feature-based priority remains less understood.

Previous research has shown that attending to a feature modulates neural activity in early visual areas, for example, by enhancing (or suppressing) activity in neurons tuned to the attended (or unattended) features (Martinez-Trujillo and Treue, 2004). More recent studies have further shown that activity in frontoparietal areas also exhibits feature-specific modulations. For example, human fMRI studies have shown that neural activity patterns can be used to decode the attended feature in both visual and frontoparietal areas (Greenberg, Esterman, Wilson, Serences, & Yantis, 2010; Kamitani & Tong, 2006; Liu, Hospadaruk, Zhu, & Gardner, 2011; Serences & Boynton, 2007). Previous work thus indicates that feature-based priority is represented at multiple levels of the visual processing hierarchy. An important open question is whether this multi-level representation

of feature-based priority accomplishes specialized or similar functions during attentional selection.

In the broad literature on brain information processing, an overarching framework is that sensory information is processed along hierarchical stages starting with analog representations and gradually progressing to more abstract representations (Deco & Rolls, 2004; Hochstein & Ahissar, 2002; Riesenhuber & Poggio, 1999). Thus, neural representations in early visual areas should reflect fine-grained information of sensory stimuli, whereas different frontoparietal areas may represent sensory stimuli at different levels of abstractness. Although these areas did not exhibit obvious functional differences in previous studies (nor was that the aim of these studies), it is possible that their contributions to attentional selection are different and complementary. To assess the level of abstractness in their representations of attentional priority, we examined how neural signals tracks feature similarity along the frontoparietal network. The rationale is that more abstract representations should be tuned less to changes in physical properties but more to high-level information such as task rules and choice categories (Freedman, Riesenhuber, Poggio, & Miller, 2001; Li, Ostwald, Giese, & Kourtzi, 2007; Swaminathan & Freedman, 2012).

In a functional magnetic resonance imaging (fMRI) study, we presented two superimposed moving dot fields (leftward and rightward) at the same location and cued subjects to selectively attend to one of the directions. The feature similarity was manipulated by varying the angular separation (30°, 90°, 150°) between the two motion directions. We performed multivariate analyses to assess the similarity between neural signals associated with attending to leftward and rightward directions. Thus, within each angular separation, the physical stimulus was kept constant while only attentional instructions varied, such that neural effects should reflect attentional modulations. Across angular separations, we examined the influence of feature similarity on multivariate measures of attentional modulation. If a brain area represents the attended feature in a *continuous* way, the neural patterns should be tuned to feature similarity, such that the neural patterns would become more different for large angular separation (attend +75° vs. attend -75°) than small angular separation (attend +15° vs. attend -15°). Alternatively, if a brain area represents the attended feature in a *discrete* way, the neural patterns should be tuned to abstract information (leftward vs. rightward), such that the patterns would be invariant to the feature similarity. Our results showed both continuous and discrete representations of the attended feature in different sub-regions of the frontoparietal network, suggesting functionally specialized neural coding of feature-based attentional priority along the cortical hierarchy.

Materials and methods

Participants

Twelve individuals (six females) participated in the experiment. We based our sample size on previous studies using similar attention tasks (Baldauf & Desimone, 2014; Guo, Preston, Das, Giesbrecht, & Eckstein, 2012; Jigo, Gong, & Liu, 2018; Liu & Hou, 2013). All had normal or corrected-to-normal vision. Eleven were right-handed and one was left-handed. One of the participants was the author (MG) and the rest were undergraduate and graduate students at Michigan State University. Participants were paid for their participation at $20/hr and gave informed consent according to the study protocol approved by the Institutional Review Board at Michigan State University.

Stimuli and apparatus

Stimuli

Stimuli were generated using MGL (http://gru.stanford.edu/mgl), a set of custom OpenGL libraries implemented in Matlab. The stimulus aperturewas an annulus with an inner radius of 1.5° and an outer radius of 6°, centered on the fixation cross on a black background. In the aperture, two superimposed dot fields were presented (dot size: 0.1°, density: 2.5 dots/degree^2). One of the dot fields moved along the leftward direction, while the other one moved along the rightward direction. The two motion directions were equally offset from the upward direction. There were three offset conditions that varied in the angular separations between the two directions: 30°, 90°, and 150° (see Figure 1(a)). When a dot moved out of the aperture, it was wrapped around to reappear from the opposite side along its motion direction.

Display

The stimuli were presented on a CRT monitor (resolution: 1024 × 768, refresh rate: 60 Hz) in the behavioral practice session. Participants were stabilized with a chinrest and viewed the display from a distance of 91 cm in a dark room. During the fMRI scans, stimuli were projected on a rear-projection screen located in the scanner bore by a Hyperion MRI Digital Projector (Psychology Software Tools, Sharpsburg, PA). The resolution and refresh rate were the same as the CRT monitor. Participants viewed the screen via an angled mirror attached to the head coil at a viewing distance of 60 cm.
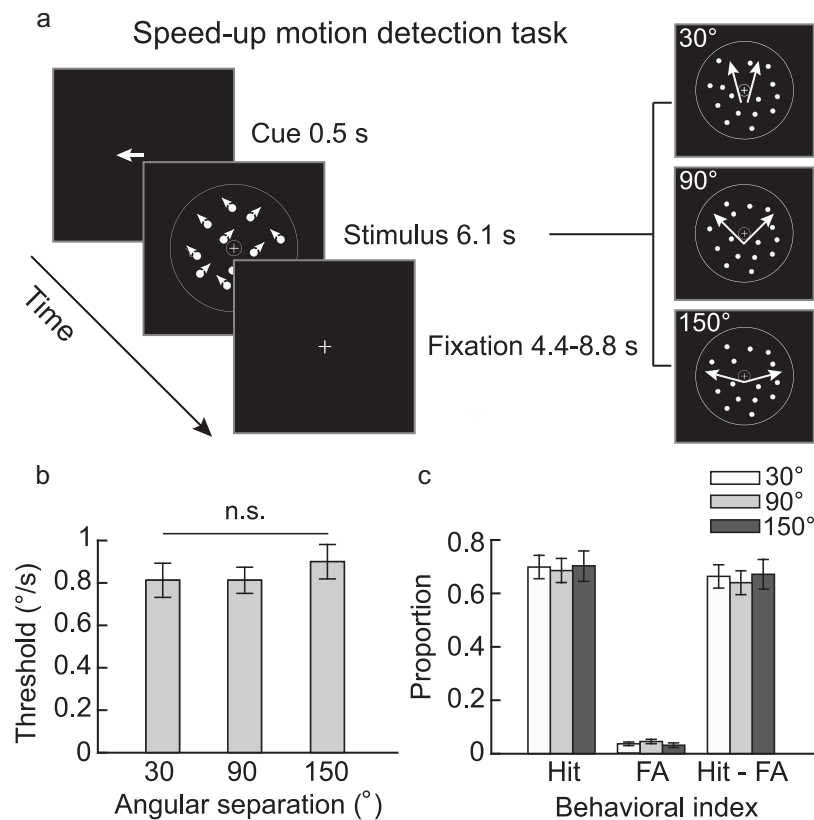
Eye tracking

To evaluate the stability of fixation, we monitored each participant's eye position during the task in the practice session. Six of the 12 participants had their eyes monitored inside the scanner as well. We used an Eyelink 1000 system (SR Research) to record the right eye in both the practice and scanning sessions. The eye tracking data were analyzed offline using custom Matlab code.

Experimental design

Task

Participants were cued to attend one of the motion directions and to perform a speed-up detection task (Figure 1(a)). At the beginning of each trial, an arrowhead (←, →) was presented for 0.5 s that instructed the participants to attend either leftward or rightward direction. The two superimposed dot fields were then presented for 6.1 s, which was followed by a fixation display varying from 4.4 s to 8.8 s (in a step size of 2.2 s). During the stimulus display, a brief speed increment lasting for 0.3 s appeared at a random interval (ranging from 1.5 to 5.8 s after the stimulus onset). The onsets of the speed-up were randomized independently for two motion directions. Thus, each

Figure 1. Trial sequence and behavioral results in the attention task. (a) The arrow cue indicated the attended motion direction (leftward vs. rightward) in the subsequent display, which was comprised of two superimposed moving dot fields. There were three possible angular separations between two motion directions: 30°, 90°, and 150° (shown on the right). The depicted trial is a 'attend to leftward' trial. The white circles demarcate the annulus-shaped aperture of the dots; they were not shown in the actual stimuli. (b) Task performance across the conditions of angular separation, as indexed by the threshold. (c) Proportion of hit and false alarm trials. Error bars are within-subject standard errors (s.e.m.), using the method by Cousineau (2005).

speed-up trial contained either a single speed-up in one of the motion directions or two speed-ups separately in each direction. Participants were instructed to respond to the speed-up in the attended direction by pressing a button and ignore the speed-up in the unattended one. A correct response was defined as a button press within 1.5 s after the onset of speed-up in the cued direction. We presented a colored dot at the center for 0.3 s immediately after a response was made. A green dot indicated a fast (<1.1 s after speed-up onset) and accurate response, a yellow dot indicated a slow (1.1–1.5 s after speed-up onset) and accurate response. An incorrect response including a false alarm or miss (>1.5 s after a speed-up) was indicated by a red dot.

Before the scanning session, we trained participants to become familiar with the task in a separate practice session. The magnitude of speed increment for each angular separation was adjusted by best PEST, as implemented in the Palamedes Toolbox (Prins and Kingdon 2009), to maintain the performance level at 71%. The proportion of speed-up trials in the practice session was 50% to accelerate the convergence of threshold estimates. The proportion of speed-up trials in the scanning session was set at 20% as our main fMRI analysis was based on trials without speed-ups. Participants were made aware of the proportion of speed-ups in both sessions.

Design

There were two within-subject factors: attended direction (leftward vs. rightward direction) × angular separations (30°, 90°, 150°). Each run contained five trials per condition (30 trials per run). Each participant completed at least 5 runs in the practice session and 11 runs in the scanning session.

MRI data acquisition

Imaging was performed on a GE Healthcare 3 T Sigma HDx MRI scanner, equipped with an eight-channel head coil, in the Department of Radiology at Michigan State University. For each participant, high-resolution

anatomical images were acquired using a T1-weighted magnetization-prepared rapid-acquisition gradient echo sequence (field of view, 256 × 256 mm; 180 sagittal slices; 1 mm isotropic voxels). Functional images were acquired using a T2* – weighted echo planar imaging sequence (repetition time, 2.2 s; echo time, 30 ms; flip angle, 78°; matrix size, 64 × 64; in-plane resolution,
3 × 3 mm; slice thickness, 4 mm, interleaved, no gap). Thirty axial slices covering the whole brain were collected. In each scanning session, we also acquired a 2D T1-weighted anatomical image that had the same slice prescription as the functional scans but with higher in-plane resolution (0.75 × 0.75 × 4 mm). The image was used to align the functional data to the high-resolution anatomical images for each participant.

Retinotopic mapping

For each participant, we ran a separate scanning session of retinotopic mapping. To define visual and parietal areas that showed topographic organization, participants viewed four runs of rotating wedges (i.e., clockwise and counterclockwise) and two runs of rings (i.e., expanding and contracting) to map the polar angle and radial components, respectively (DeYoe et al., 1996; Engel, Glover, & Wandell, 1997; Sereno et al., 1995). Borders between areas were defined as the phase reversals in a polar angle map of the visual field. Phase maps were visualized on computationally flattened representations of the cortical surface, which were generated from the high-resolution anatomical image using FreeSurfer (http://surfer.nmr.mgh.harvard.edu) and custom Matlab code.

To help identify the topographic areas in parietal areas, we ran 2–4 runs of memory-guided saccade task developed in previous studies (Sereno, Pitzalis, & Martinez, 2001; Schluppeck et al. 2006; Konen and Kastner 2008b). Participants fixated at the screen center while a peripheral (~10° radius) target dot was flashed for 500 ms. The flashed target was quickly masked by a ring of 100 distractor dots randomly positioned within an annulus (8.5–10.5°). The mask remained on screen for 3 s, after which participants were instructed to make a saccade to the memorized target position, then immediately saccade back to the central fixation. The position of the peripheral target shifted around the annulus from trial to trial in either a clockwise or counterclockwise order. Data from the memory-guided saccade task were analyzed using the same phase encoding method as the wedge and ring data.

In addition, one run consisted of alternating moving versus stationary dots was used to localize the motion-sensitive area, MT+, an area near the junction of the occipital and temporal cortex (Watson et al., 1993).

Therefore, the following regions of interest (ROIs) in each hemisphere were identified after the completion of this session: V1, V2, V3, V3A/B, V4, V7, MT+, IPS1 to IPS4.

fMRI data analysis

Preprocessing

Data analyses were performed using mrTools (http://www.cns.nyu.edu/heegerlab/wiki/doku.php?id=mrtools:top) and custom code in Matlab. For each run, functional data were preprocessed with head motion correction, linear detrending and temporal high pass filtering at 0.01 Hz. Data were converted to percentage signal change by dividing the time course of each voxel by its mean signals in each run. Data from 11 runs were concatenated for further analysis. Importantly, we analyzed trials without speed-ups and trials on which participants did not make button press responses. This yielded on average ~254 trials per participant (~42 trials per condition).

Univariate analysis: Deconvolution

We used a deconvolution approach by fitting each voxel's time series with a general linear model whose regressors contained six conditions: attended direction (leftward vs. rightward) × angular separations (30°, 90° or 150°). Each trial was modeled by a set of 12 finite impulse response functions (FIR) after the trial onset (26.4 s duration). The design matrix was pseudo-inversed and multiplied by the time series to obtain an estimate of the hemodynamic response (HRF) evoked by each condition.

For each voxel, we computed goodness-of-fit measure (r^2 value), corresponding to the amount of variance explained by the deconvolution model (Gardner et al., 2005). The r^2 value represents the degree to which the voxel's response over time is correlated with the attention task. The statistical significance of the r^2 value was evaluated by a permutation test that repeated the deconvolution analysis with shuffled trial labels (Gardner et al., 2005; Liu et al., 2011). The p value of each voxel was calculated as the percentile of voxels from the null (permutated) distribution that exceeded the observed r^2 value. We selected voxels from the retinotopically defined ROIs that exceeded the r^2 value at a cutoff p value of 0.01. In addition, we excluded noisy voxels with responses larger than 10% signal change at any time point in the time series. The selected voxels were used for both univariate and multivariate analysis. The exact exclusion criterion did not qualitatively impact our results.

Using the r^2 value, we defined three additional areas that were active during the attention task, separately for each hemisphere: frontal eye field (FEF), inferior frontal junction (IFJ) and anterior branch of intraparietal areas that likely corresponds to IPS5, which is anatomically
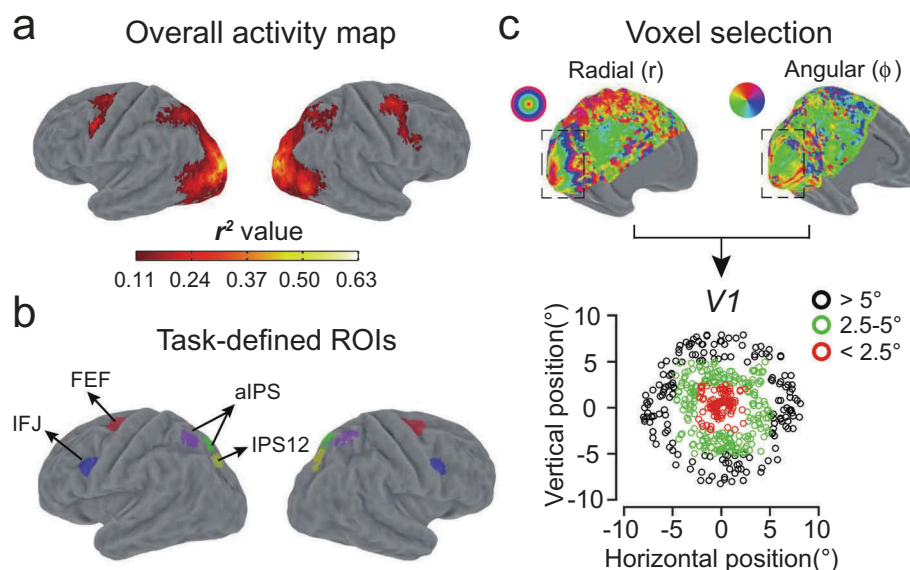
anterior and lateral to IPS4 (Konen and Kastner, 2008b; Wang et al., 2015). All ROI-based analyses were performed in each participant's native anatomical space. For each ROI and each condition, we calculated the response amplitude by averaging a time window of 2.2–15.4 s (2nd to 8th time points after trial onset) of the deconvolved fMRI responses, a period of time that the response showed elevated response above baseline. To visualize the overall activation pattern during the task, we transformed individual r^2 map to the Population-Average, Landmark- and Surface-based (PALS) atlas (Van Essen, 2005) using spherical alignment. We then averaged the maps and thresholded with an r^2 value of 0.11 in combination with a cluster constraint of 50 voxels (Figure 2(a)). Note this group analysis was performed for the purpose of visualization only. To visualize the locations of frontoparietal ROIs, we overlaid individually defined ROIs in the atlas surface and displayed the vertices shared across the majority of the hemispheres (Figure 2(b)).

Multivariate analysis: Voxel selection

Previous research has shown that voxels responding to the stimulus aperture edge in early visual areas exhibit a large-scale bias for motion directions (Wang et al. 2014). To eliminate the contribution of such bias to motion decoding, we excluded the voxels that responded to the edge of the apertures in V1 to V3 using the retinotopy data. For each voxel in these areas, we used its radial component (acquired from runs of expanding and contracting rings) and polar angle component (acquired from runs of rotating wedges) to calculate its response field location (Figure 2(c)). We included voxels whose response field location was within 2.5–5°, which excluded the inner and outer edges of the stimulus apertures.

In addition to excluding edge-related voxels in early retinotopic areas, we also selected active voxels based on their univariate responses. For each subject, we selected the same number of voxels with top-ranked r^2 values in each ROI. The exact number of voxel was individually defined as the minimal number of voxels across ROIs for that particular subject. This voxel selection regime controlled for potential biases in multivariate analyses due to varying number of voxels across regions, and it also took into account the inter-subject variability in overall ROI sizes. Due to the relatively small number of voxels in each sub-region of IPS, we combined IPS1 and IPS2 to form a posterior IPS (IPS12), and combined IPS3 and IPS4 and anterior branch of IPS to form an anterior IPS (aIPS) according to their functional similarities (Konen and Kastner 2008a). This criterion yielded on average 80 voxels per ROI (SD = 20.9) for the multivariate analyses across subjects. We note that our results are not sensitive to the exact voxel selection criterion; the same qualitative results were obtained with other criteria such as using all voxels per ROI.

Figure 2. (a) The group-averaged r^2 map shown on an inflated Caret atlas surface. Individual maps were transformed to PALS atlas space and averaged, which was thresholded at r^2 value of 0.11 with a cluster constraint of 50 voxels. (b) Average frontoparietal ROI locations. For each ROI, the vertices shared by more than half of the hemispheres (n > 6) are displayed. IPS: intraparietal sulcus, FEF: frontal eye field, IFJ: inferior frontal junction. (c) Voxel selection for multivariate pattern analysis in early visual areas (V1–V3). (*Left*) An example of selected voxels in V1 of an individual hemisphere. Each colored dot corresponds to a single voxel's response field location in the visual field, which was calculated based on voxels' angular and radial component estimated from retinotopic mapping (*Right*). The voxels represented by green colored dots were included for multivariate analyses, thus excluding voxels responding to the inner and outer edges of the stimulus annulus (shown by red and black dots, respectively).

Multivariate analysis: Classification accuracy

For each voxel and each trial, we obtained an fMRI response amplitude by averaging a time window of 4.4–8.8 s after trial onset (3rd to 5th time points). This averaging window was used to account for the hemodynamic delay and avoid signal contribution from adjacent trials. Note that we chose different time points for univariate and multivariate analysis because these two types of analysis relied on different data inputs. The univariate analysis was based on the deconvolved response (with a GLM model), whereas here we simply extracted time points corresponding to each trial from the raw time series for multivariate analysis (e.g., Kamitani & Tong, 2006; Serences & Boynton, 2007). For decoding of attention, we normalized the response amplitudes across the two attention conditions (attend leftward vs. attend rightward direction) using a z-score, separately for each angular separation. For decoding of stimulus, we normalized the response amplitudes across two stimulus conditions (e.g., 30° and 90°) using z-score, separately for all pairwise combinations. We applied MVPA on normalized response amplitudes from trials without manual responses (~42 trials per condition, see above). We trained the classifier to discriminate between two attention conditions (attend leftward vs. attend rightward direction) using the Fisher linear discriminant analysis.

The discriminant function can be expressed by a weighted sum of voxel responses plus a bias:

$$g(x) = \sum_{i=1}^{n} w_i x_i + w_0$$

where n is the number of voxels, w_i and x_i are the weight and response of the ith voxel, and w_0 is the bias point. We divided the data set into training (10 runs) and testing data (1 run). For each angular separation, we used the training data to find optimal weights and bias point for the discriminant function, and then evaluated the discriminant function on the testing data in an 11-fold leave-one-run-out cross-validation scheme. For this analysis, we used classification accuracy (i.e., proportion of correctly classified trials averaged across folds) to index neural pattern difference between the two attention conditions, as a larger pattern difference should yield higher accuracy.

Multivariate analysis: Class separation (via Mahalanobis distance)

Because classification can be construed as a discretized readout of the pattern difference on individual trials, it might affect our ability to evaluate continuous vs. discrete neural representations by masking subtle pattern differences. Thus, as a complementary analysis, we calculated the Mahalanobis distance (Mahalanobis, 1936) to quantify the class separation between two attention conditions as a function angular separation. Mahalanobis distance is a continuous measure of pattern difference between two multivariate distributions (Mahalanobis, 1936), which is similar to Euclidean distance except that the variance of each voxel and the covariance between voxels were considered. Similar to the inputs for classification, we calculated the Mahalanobis distance on the basis of normalized response amplitudes. We used data from all 11 runs to calculate a single Mahalanobis distance for each angular separation condition in each ROI. The (squared) Mahalanobis distance is defined by

$$MD^2 = (\vec{\mu_2} - \vec{\mu_1})^T \, \Sigma^{-1} (\vec{\mu_2} - \vec{\mu_1})$$

where MD is the Mahalanobis distance, $\vec{\mu_1}$ and $\vec{\mu_2}$ are the mean response vectors of two attention conditions, T denotes transposition, and Σ is the combined covariance matrix for the two conditions. Because the covariance matrix would be underdetermined with more voxels than trials, we therefore used a regularized version of the covariance matrix by adding a ridge coefficient to the diagonal elements of combined covariance matrix (Warton, 2008).

Statistical analysis

Behavior data

For the speed-up detection task, we conducted one-way repeated-measures analysis of variance (ANOVAs) with angular separation as the factor. For the eye movement data, we averaged participants' eye position during the stimulus period (0 to 6.6 s) in each trial and conducted two-way repeated-measures ANOVAs (attended direction × angular separation), both for group-level (using mean and standard deviation of eye position across trials for each participant) and subject-level (using mean and standard deviation of eye position across time on each trial) analysis.

Neural data

To test if our experimental manipulation induced changes in overall BOLD response, we performed two-way repeated-measures ANOVAs (attended direction × angular separation) on the averaged fMRI response amplitude obtained from univariate analysis. To map out areas containing attentional signals along the visual hierarchy, we collapsed data across angular separations for each brain area and performed separate one-sample t-tests (against the 0.5 chance-level) on the multivariate decoding results.

To characterize the representational properties (continuous vs. discrete) of the attended feature, we performed one-way repeated-measures ANOVAs (angular separation) on the two measures of pattern difference (classification accuracy and class separation) for separate brain areas. To streamline the data presentation, we aggregated data from extrastriate visual areas (abbreviated as ExS) by averaging results across V2, V3, V3A/B, V4, and V7, which did not show qualitative differences when inspected individually. We kept V1 and MT+ as separate visual ROIs because of the importance of former's role in early visual processing and the latter's role in motion processing. We further conducted trend analyses to explore whether the effect of angular separation can be explained by a linear or quadratic component. As our pre-defined ROIs have been repeatedly reported in the literature, there are strong priors for planned statistical tests on these areas. Nevertheless, our statistical inferences remain essentially the same if we use the false discovery rate (FDR) method (Benjamini & Hochberg, 1995) to correct for multiple comparisons across areas.

We also conducted Bayesian repeated-measures ANOVA using JASP (JASP team, 2017), particularly for ROIs that showed invariant activity with respect to changes in the angular separation. The Bayes factor (BF_{01}) indexes the strength of evidence that the data favor the null hypothesis compared to the alternative hypothesis, as a complement to the p-values in standard null-hypothesis significance test.
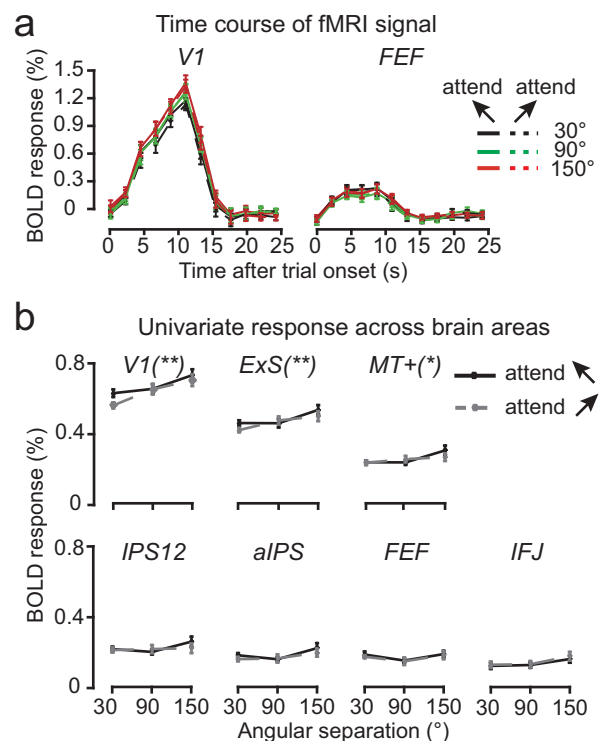
Results

Behavioral performance

Behavioral performance on the speed-up detection task confirmed that the participants were selectively attending to one of the dot fields. The task difficulty remained at an intermediate level across conditions and participants. The hit rate for speed-up was around 70% and false alarm (FA) rate was less than 5% (Figure 1(b)). One-way ANOVAs were performed on multiple behavioral indices across three angular separations, which showed no significant main effects for hit rate ($F(2,22) = 0.04$, $p = 0.96$), false alarm rate ($F(2,22) = 0.88$, $p = 0.43$), and hit – false alarm rate ($F(2,22) = 0.13$, $p = 0.88$). In addition, the speed-up threshold also did not differ among conditions ($F(2,22) = 1.96$, $p = 0.16$). These results demonstrated that there were no discernible differences in behavior across angular separations, which is expected given our experimental design that explicitly controlled performance with a staircase method.

Univariate analysis: Response amplitude

To determine whether there were any overall modulations in neural response across conditions, we compared the mean response amplitude across conditions for each ROI. Figure 3(a) shows time courses of fMRI response in two selected regions (V1 and FEF). We observed robust fMRI responses for all conditions in all areas. In visual areas, there was a small but systematic modulation such that larger angular separations tend to evoke larger responses. We first examined the potential difference between hemispheres and if such a difference interacted with the attended direction (leftward vs. rightward). We did not find any statistically reliable effects. Thus for all univariate results, we collapsed across the two hemispheres and performed two-factor ANOVAs to quantify the effects of angular separation and attended direction (Figure 3(b)). We found significant main effects of angular separation in V1 ($F(2,22) = 9.64$, $p < 0.001$, $\eta_p^2 = 0.473$), ExS ($F(2,22) = 7.02$, $p < 0.001$, $\eta_p^2 = 0.552$), and MT+ ($F(2,22) = 3.65$, $p = 0.043$, $\eta_p^2 = 0.261$). In contrast, response amplitude in frontoparietal areas was not affected by the changes in the angular separation ($p > 0.10$ all for frontoparietal areas). Additionally, neither attended direction ($p > 0.36$ for all areas) nor the two-factor interaction ($p > 0.24$ for all areas) was significant in any ROIs. To further ascertain if visual and frontoparietal areas behaved differently in response to the

Figure 3. (a) Mean fMRI time course from two representative regions (V1 and FEF). Error bars denote within-subject s.e.m. across all time points. (b) Mean fMRI responses in visual and frontoparietal areas for each condition (attended direction × angular separation). Error bars denote within-subject s.e.m. Significant level for the difference across angular separation is indicated by symbols (**$p < 0.01$, * $p < 0.05$).

angular separation, we formed two region groups (visual vs. frontoparietal) by averaging the response amplitude within visual (V1, ExS and MT+) and frontoparietal (IPS12, aIPS, FEF, and IFJ) areas. A three-way ANOVA (region group × angular separation × attended direction) revealed a significant interaction between region group and angular separation (F(2,22) = 20.67, $p < 0.001$, $\eta_p^2 = 0.653$), demonstrating visual areas are more sensitive to changes in angular separation than frontoparietal areas.

Multivariate analysis: Classification accuracy and neural separation

We examined the neural representation of attentional priority by decoding the attended feature from multivoxel response patterns (Kamitani & Tong, 2006; Liu et al., 2011). Average decoding accuracy across angular separations showed above-chance performance in all ROIs (one sample t-test, $ps < 0.019$). Thus, our result showed reliable neural representations of attended feature along the visual hierarchy, making it meaningful to further test the modulation of the feature similarity on these representations. To facilitate the exposition, below we present results from the occipital visual areas (V1, ExS, and MT+) and frontoparietal areas (IPS12, aIPS, FEF, and IFJ) separately.

Neural pattern difference in visual areas: Dominance of continuous representation

We used two measures to evaluate pattern difference as a function of feature similarity: classification accuracy and class separation (see Materials and Methods for details). Because of the well-established precise feature tuning in visual areas, we expected these areas to exhibit continuous representations (i.e., neural patterns should become more similar when the angular separation between the attended directions decreases).
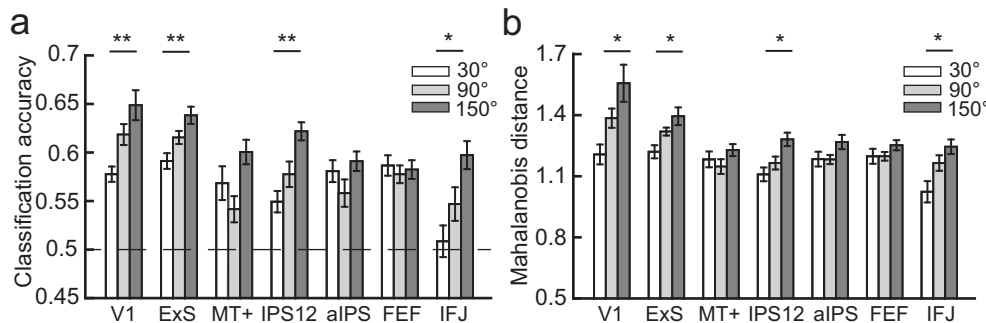
Classification accuracy

We performed separate one-way repeated-measures ANOVAs across angular separation to test whether feature similarity impacts the classification accuracy in each visual ROI (Figure 4(a)). The results showed significant effect of angular separation in V1 (F(2,22) = 6.12, $p = 0.008$, $\eta_p^2 = 0.357$) and ExS (F(2,22) = 5.86, $p = 0.009$, $\eta_p^2 = 0.348$). Trend analyses in these areas further revealed significant linear ($ps < 0.013$), but no quadratic components ($ps > 0.75$), indicating a monotonic relationship between the classification accuracy and angular separation. There were no significant effects of angular separation in MT+ (F(2,22) = 2.71, $p = 0.089$, $\eta_p^2 = 0.198$).

Class separation (Mahalanobis distance)

We performed the same repeated-measures ANOVAs to test the modulation of feature similarity on the class separation as indexed by Mahalanobis distance. The results were essentially the same to those from the classification accuracy (Figure 4(b)). The class separation increased when the attended features became more dissimilar in V1 (F(2,22) = 4.73, $p = 0.020$, $\eta_p^2 = 0.30$) and ExS (F(2,22) = 4.65, $p = 0.021$, $\eta_p^2 = 0.297$). Trend analysis in these ROIs showed linear ($ps < 0.04$), but no quadratic component ($ps > 0.69$). There were no significant effects of angular separation in the MT+ ($p = 0.422$).

Results from both classification accuracy and class separation consistently showed an increased pattern difference with larger angular separation in early visual areas, consistent with their established role in processing fine-grained sensory inputs. The trend analysis further demonstrated that the pattern difference shows a monotonic increase with angular separation in V1 and ExS. The lack of feature similarity effect in MT+ is somewhat unexpected given its prominence in motion processing. However, the overall classification accuracy in MT+ (57.0%) tended to be lower than that in visual areas (V1 and ExS) (61.5%), consistent with prior fMRI studies (e.g., Kamitani & Tong, 2006;

Figure 4. Multivariate results for attention decoding as a function of feature similarity. (a) Classification accuracies for the attended direction in visual and frontoparietal ROIs. (b) Class separation between the two attended directions in visual and frontoparietal ROIs. Significant level for the difference across angular separation is indicated by symbols (**$p < 0.01$, * $p < 0.05$). Error bars are within-subject s.e.m.

Serences & Boynton, 2007). This has been attributed to the possibility of closely spaced direction-selective columns in this area that decreases the spatial inhomogeneity for fMRI-based pattern analysis (Bartels, Logothetis, & Moutoussis, 2008; Kamitani & Tong, 2006). In addition, it is also possible that signals in MT+ are dominated by low-level effects related to motion processing, which could limit our ability to detect changes in attentional modulations.

Neural pattern difference in frontoparietal areas: Mixed representation of attentional priority

Classification accuracy

We performed separate one-way repeated-measures ANOVAs to test whether feature similarity impacts the classification accuracy in parietal (IPS12 and aIPS) and frontal (FEF and IFJ) ROIs. This analysis revealed a significant main effect of angular separation in IPS12 ($F(2,22) = 7.03$, $p= 0.004$, $\eta_p^2 = 0.390$) and IFJ ($F(2,22) = 5.13$, $p= 0.015$, $\eta_p^2 = 0.318$), which can be accounted by a linear trend ($ps<0.006$), but not a quadratic trend ($ps>0.69$). However, decoding in aIPS and FEF were not influenced by the changes in angular separations ($ps>0.28$). These results suggest functional distinctions in frontoparietal areas, which was further supported by a direct test for interactions across subregions in this network: a two-way repeated-measures ANOVA (ROI × angular separation) showed a significant interaction effect ($F(6,66) = 3.64$, $p = 0.004$, $\eta_p^2 = 0.249$).

Class separation (Mahalanobis distance)

The repeated-measures ANOVAs on the class separation revealed a significant increase when the attended feature became more dissimilar in IPS12 ($F(2,22) = 4.79$, $p= 0.019$, $\eta_p^2 = 0.30$) and IFJ ($F(2,22) = 4.59$, $p= 0.022$, $\eta_p^2 = 0.294$). Again, the trends of the effects in IPS12 and IFJ were linear ($ps<0.02$), not quadratic ($ps>0.53$). The class separation in aIPS and FEF were little affected by the angular separations ($ps>0.22$). The same two-way repeated-measures ANOVA (ROI × angular separation) was conducted on the class separation and showed a significant interaction effect ($F(6,66) = 3.08$, $p = 0.01$, $\eta_p^2 = 0.219$).
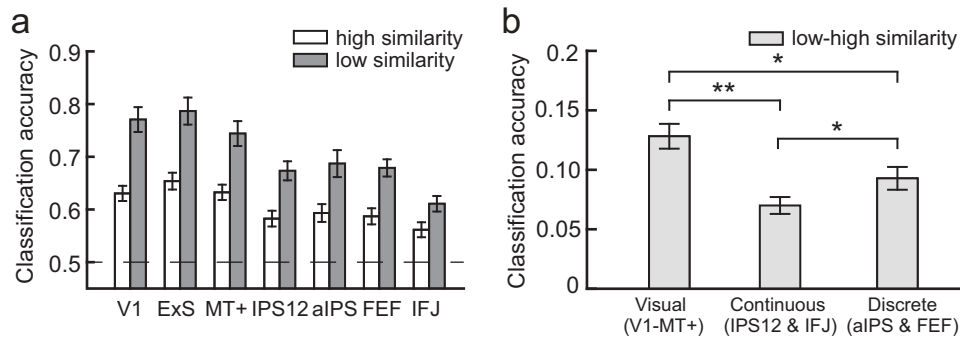
Bayesian analysis

We further used the Bayesian approach (Wagenmakers, 2007) to assess the relative evidence between the null and alternative hypotheses in areas that showed a lack of effect of angular separation: aIPS and FEF. Bayesian repeated-measures ANOVAs were performed in each of these ROIs for both classification accuracy and class separation (see Materials and Methods). As quantified

by BF_{01}, the null model was preferred to the alternative model in aIPS (classification accuracy: 4.89; class separation: 4.06) and FEF (classification accuracy: 13.08; class separation: 7.44). The Bayesian analysis thus offered support for the invariance of attentional signals across levels of feature similarity in these areas.

Neural representation of attention was not contributed by stimulus sensitivity

Although we used superimposed stimuli to equate sensory inputs and only varied attention instructions within each angular separation, the effect of feature similarity was assessed by comparing across different stimuli, which could introduce stimulus-driven effect in our measure of attentional priority. Specifically, the observed difference between continuous and discrete representations of attentional priority could be related to differential sensitivity to stimulus information across areas, such that areas more sensitive to stimulus difference also exhibit a more continuous representation of attentional priority. To test this possibility, we conducted an additional analysis that compared stimulus decoding across areas and focused on frontoparietal areas showing continuous (IPS12 and IFJ) and discrete (aIPS and FEF) representations.

We performed explicit stimulus decoding by training a classifier to decode between physical stimuli, for stimulus pairs of high similarity (30° vs. 90° and 90° vs. 150°) and low similarity (30° vs. 150°). We averaged the two attention conditions for each stimulus for this analysis. For example, when classifying 30° vs. 90°, we averaged BOLD response for attend +15° and attend -15° conditions to obtain data for 30°, and we averaged attend +45° and attend -45° conditions to obtain data for 90°. Because we averaged data from the two attention conditions, feature-specific attention effect should be averaged out and results should reflect stimulus-driven effects. Neural signals sensitive to stimulus difference should show a difference in decoding accuracy for low similarity and high similarity conditions. Indeed, we observed higher decoding accuracies for low vs. high similarity in all areas (Figure 5(a), paired t-tests, $ps<0.01$), demonstrating the sensitivity to stimulus information. We thus used this difference to index neural sensitivity to stimulus difference, and compared average difference in three ROI groups: visual areas (V1, ExS and MT+), frontoparietal areas with continuous (IPS12 and IFJ) and discrete representation (aIPS and FEF) of attentional priority (Figure 5(b)). One-way repeated-measures ANOVA revealed a significant main effect of ROI group ($F(2,22) = 14.92$, $p< 0.01$, $\eta_p^2 = 0.576$). Visual areas exhibited a higher stimulus sensitivity than frontoparietal areas ($ps<0.02$), which is

Figure 5. Multivariate results for stimulus decoding as a function of stimulus difference. (a) Classification accuracies for stimulus pairs of high similarity (average of 30° vs. 90° and 90° vs. 150°) and low similarity (30° vs. 150°). (b) Mean difference of classification accuracy between high and low similarity stimulus pairs in visual areas, frontoparietal areas with continuous (IPS12 and IFJ) and discrete (aIPS and IFJ) representation. The significance level for the regional difference is indicated by symbols (**$p < 0.01$, * $p < 0.05$). Error bars are within-subject s.e.m.

expected because of the fine feature tuning in these areas. Critically, continuous areas showed lower stimulus sensitivity than discrete areas (p = 0.013). Thus, although frontoparietal areas all exhibited some degree of stimulus sensitivity, differential sensitivity cannot explain the observed difference in continuous vs. discrete representation of attentional priority.

Eye movement cannot account for the fMRI results

To examine whether any differences in eye movement patterns can explain our results, we analyzed the participants' mean eye position and spread of fixation (as quantified by the standard deviation of fixations) in both the training session and scanning session (see Materials and Methods). For group-level analysis, a two-factor ANOVA (attended direction × angular separation) on the mean and standard deviation of fixation position showed neither significant main effects nor interaction in either session ($ps > 0.17$ for all analysis). We also conducted similar analysis for each individual subject on trial-level data. None of the subjects showed significant differences across conditions ($ps > 0.10$ for all comparisons). We thus conclude that eye movement cannot account for our observed fMRI results.

Discussion

Previous studies have highlighted the neural representation of attentional priority of features along the cortical hierarchy (e.g., Ibos & Freedman, 2014; Jigo et al., 2018; Liu et al., 2011). In the present study, we addressed whether the functions of frontoparietal regions are specialized or similar during attentional selection. By characterizing the distributed neural activity (using both classification accuracy and class separation) as a function of feature similarity, we identified two distinct profiles of attentional

priority signals in frontoparietal areas. In posterior IPS (IPS12) and IFJ, neural pattern difference increased when the attended features became more distinct, indicating a continuous representation of attentional priority. Similar effects were also found in visual areas (V1 and ExS). Conversely, in more anterior parts of IPS and FEF, neural pattern difference remained constant regardless of the changes in feature similarity, indicating a discrete representation of attentional priority. The functional dissociation across sub-regions of frontoparietal areas suggests two complementary ways that the brain uses to represent feature-based attentional priority. We further ruled out the possibility that our findings were contributed by different degrees of stimulus sensitivity across brain areas.

We found that the mean fMRI BOLD amplitude was sensitive to changes in the similarity between the two directions (30°, 90° and 150° separation) in visual areas, but not in frontoparietal areas. In visual areas, when the two directions became more distinct, the compound stimulus likely activated more distinct subpopulations of direction-selective neurons, leading to an overall larger BOLD response. This reflected a pure stimulus-driven effect and was absent in frontoparietal areas where neurons were less tuned to physical properties of the stimulus. That the mean response amplitude reflected stimulus-driven effect was also supported by the observation that it was insensitive to the attended direction (leftward vs. rightward). However, information about the attended direction, or attentional priority, can be decoded from the distributed pattern of neural activity, consistent with previous studies (Kamitani & Tong, 2006; Liu, 2016; Liu et al., 2011; Serences & Boynton, 2007).

We found attentional priority in visual areas, as measured by the multivariate decoding, was modulated by feature similarity, such that the neural patterns became more different with larger angular separations. This is

likely caused by attentional modulation occurring on more distinct direction-selective neuronal subpopulations at larger angular separations, which led to more distinct spatial activity patterns. We note that MT+ did not show such a modulation, which could be related to its overall low decoding accuracy due to the anatomical organization and/or the relative contribution of stimulus-driven vs. attentional effects in this area (see Results). The continuous representation of the attended features in visual areas is in line with the general framework that neurons in visual areas encode precise visual properties and subject to attentional modulation, whereas the source of such top-down modulations likely resides in control regions, such as areas in the frontoparietal cortex (Bisley & Goldberg, 2010; Kastner & Ungerleider, 2000). Our finding of mixed neural signals with both continuous and discrete representations for feature-based priority thus suggests a further fractionation of functions in this network.

In posterior IPS and IFJ, we found neural signals that coded for physical variations of attended features, in a similar manner as those observed in visual areas. These findings are consistent with the role of posterior IPS as a key integrator of top-down and bottom-up information (Bisley & Goldberg, 2010) during attentional selection, which may be functionally associated with the build-up of precise attentional templates that enables the efficient selection among similar items, as has been demonstrated to be behaviorally feasible (Navalpakkam & Itti, 2006). Previous work from others and our lab has provided some support for this potential neural-behavioral link for posterior IPS (Law and Gold, 2008; Jigo et al., 2018). Previous studies have also supported a general role of IFJ in cognitive control (Brass, Derrfuss, Forstmann, & von Cramon, 2005; Zanto, Rubens, Bollinger, & Gazzaley, 2010), with more recent studies identifying IFJ as a source of feature and object-based selection (Baldauf & Desimone, 2014; Bichot, Heard, DeGennaro, & Desimone, 2015; Zhang, Mlynaryk, Ahmed, Japee, & Ungerleider, 2018). Our results extend the function of IFJ by showing the continuous representation of attended feature in this area. This coding property may make IFJ an ideal region for sending top-down signals for particular features. Thus, despite similar representations in posterior IPS and IFJ, their exact roles may differ in terms of the source of attentional control.

In contrast to the results from posterior IPS and IFJ, the distributed neural activity in anterior parts of IPS and FEF exhibited discrete coding for the attended feature, suggesting that other regions in frontoparietal network are primarily tuned to abstract but not physical attributes of the attended feature. Given that the neural activities in these high-order areas were susceptible to task demand (Duncan, 2001; Miller & Cohen, 2001; Vaziri-Pashkam & Xu, 2017; Woolgar, Hampshire, Thompson, & Duncan, 2011),

task-specific goals or rules may well drive neural populations to represent more abstract information of the stimuli. For example, studies on category learning have shown these areas exhibit category selectivity independent of physical features (Freedman et al., 2001; Li et al., 2007; Swaminathan & Freedman, 2012). It is thus worthwhile to note that our findings of discrete signals in anterior IPS and FEF likely reflect an automatic abstraction of the attended feature because the task itself only requires simple speed detection without explicit categorization. In addition, the discrete coding cannot be explained by stimulus-response mapping, because the same response key was used for both attention conditions. Lastly, we conducted multivariate analyses only on trials without speed-ups and manual responses, further eliminating contributions from target-detection and motor response. The finding of discrete coding is consistent with the role of frontoparietal areas in mediating abstract, high-order cognitive control (Badre, 2008; Miller & Cohen, 2001). Such discrete representation could be useful in reducing the processing redundancy and enhancing the generalizability of abstract codes to other stimuli that share category-like similarity. Although we intentionally minimized possible mappings of stimuli onto explicit categories in the current task, an abstract, discrete neural code can still be useful in situations with clear alternatives (attend leftward vs. rightward directions). For example, representing ranges of directions as distinct categories may allow priority signals to be easily 'read out' by downstream areas which could facilitate attentional control.

A number of previous studies have examined the nature of neural representations in frontoparietal areas and have reached apparently different conclusions. For example, feature-independent coding of object was found in visual search (Guo et al., 2012) and face identification tasks (Jeong & Xu, 2016), whereas the continuous coding of orientation was reported in a working memory task (Ester, Sprague, & Serences, 2015) and an orientation discrimination task (Ester, Sutterer, Serences, & Awh, 2016). These studies differ greatly in stimuli, task, and analytic approaches, and thus it is difficult to pinpoint the factor that contributed to the discrepant findings. Although our study is not designed to reconcile these findings, here we offer a potential explanation based on task demand across these studies. It is possible that the task requiring precise recall of memorized item or fine discrimination in Ester et al. (2015, 2016) engaged more regions to encode detailed feature information to improve sensitivity, whereas detecting a target among distracters (Guo et al., 2012; Jeong & Xu, 2016) may sway these areas to code more abstract information pertaining to task goals. Because these latter studies did not manipulate feature similarity, it is possible that continuous feature coding co-exists with abstract

representations, as observed in our study. The present study thus extends the literature by showing both types of neural coding in frontoparietal areas, which could endow brain networks to adjust information processing flexibly across a variety of tasks. We also note that the distinction between continuous and discrete representation could very well reflect two extremes on a continuous-to-discrete continuum. Further research is needed to examine the influence of task factors on the form and the transition of neural representations in frontoparietal network.

In summary, our findings provide novel evidence for a mixture of continuous and discrete priority signals in frontoparietal network during feature-based attentional selection, revealing functional specializations in this well-studied network. This functional organization is desirable because invariance to physical changes could benefit the stable representation and recognition of stimuli, while sensitivity to fine-grained information allows selection of precise feature values, thus providing complementary representations of attentional priority to facilitate adaptive behavior in a dynamic environment.

Author contributions

T.L. and M.G. designed study; M.G. performed research and analyzed data. M.G. and T.L. wrote the paper.

Disclosure statement

No potential conflict of interest was reported by the authors.

ORCID

Mengyuan Gong http://orcid.org/0000-0003-0333-4957
Taosheng Liu http://orcid.org/0000-0002-9768-0393

References

Badre, D. (2008). Cognitive control, hierarchy, and the rostro–caudal organization of the frontal lobes. *Trends in Cognitive Sciences*, *12*(5), 193–200.

Baldauf, D., & Desimone, R. (2014). Neural mechanisms of object-based attention. *Science*, *344*(6182), 424–427.

Bartels, A., Logothetis, N. K., & Moutoussis, K. (2008). fMRI and its interpretations: An illustration on directional selectivity in area V5/MT. *Trends in Neurosciences*, *31*(9), 444–453.

Benjamini, Y., & Hochberg, Y. (1995). Controlling the false discovery rate: A practical and powerful approach to multiple testing. *Journal of the Royal Statistical Society. Series B (Methodological)*, *57*, 289–300.

Bichot, N. P., Heard, M. T., DeGennaro, E. M., & Desimone, R. (2015). A source for feature-based attention in the prefrontal cortex. *Neuron*, *88*, 832–844.

Bisley, J. W., & Goldberg, M. E. (2010). Attention, intention, and priority in the parietal lobe. *Annual Review of Neuroscience*, *33*, 1–21.

Brass, M., Derrfuss, J., Forstmann, B., & von Cramon, D. Y. (2005). The role of the inferior frontal junction area in cognitive control. *Trends in Cognitive Sciences*, *9*(7), 314–316.

Cousineau, D. (2005). Confidence intervals in within-subject designs: A simpler solution to Loftus and Masson's method. *Tutorials in Quantitative Methods for Psychology*, *1*(1), 42–45.

Deco, G., & Rolls, E. T. (2004). A neurodynamical cortical model of visual attention and invariant object recognition. *Vision Research*, *44*(6), 621–642.

Desimone, R., & Duncan, J. (1995). Neural mechanisms of selective visual attention. *Annual Review of Neuroscience*, *18*(1), 193–222.

DeYoe, E. A., Carman, G. J., Bandettini, P., Glickman, S., Wieser, J., Cox, R., … Neitz, J. (1996). Mapping striate and extrastriate visual areas in human cerebral cortex. *Proceedings of the National Academy of Sciences*, *93*(6), 2382–2386.

Duncan, J. (2001). An adaptive coding model of neural function in prefrontal cortex. *Nature Review Neuroscience*, *2*(11), 820–829.

Engel, S. A., Glover, G. H., & Wandell, B. A. (1997). Retinotopic organization in human visual cortex and the spatial precision of functional MRI. *Cerebral Cortex*, *7*(2), 181–192.

Ester, E. F., Sprague, T. C., & Serences, J. T. (2015). Parietal and frontal cortex encode stimulus-specific mnemonic representations during visual working memory. *Neuron*, *87*(4), 893–905.

Ester, E. F., Sutterer, D. W., Serences, J. T., & Awh, E. (2016). Feature-selective attentional modulations in human frontoparietal cortex. *Journal of Neuroscience*, *36*(31), 8188–8199.

Freedman, D. J., Riesenhuber, M., Poggio, T., & Miller, E. K. (2001). Categorical representation of visual stimuli in the primate prefrontal cortex. *Science*, *291*(5502), 312–316.

Gardner, J. L., Sun, P., Waggoner, R. A., Ueno, K., Tanaka, K., & Cheng, K. (2005). Contrast adaptation and representation in human early visual cortex. *Neuron*, *47*(4), 607–620.

Greenberg, A. S., Esterman, M., Wilson, D., Serences, J. T., & Yantis, S. (2010). Control of spatial and feature-based attention in frontoparietal cortex. *Journal of Neuroscience*, *30*(43), 14330–14339.

Guo, F., Preston, T. J., Das, K., Giesbrecht, B., & Eckstein, M. P. (2012). Feature-independent neural coding of target detection during

search of natural scenes. *Journal of Neuroscience*, *32*(28), 9499–9510.

Hochstein, S., & Ahissar, M. (2002). View from the top: Hierarchies and reverse hierarchies in the visual system. *Neuron*, *36*(5), 791–804.

Ibos, G., & Freedman, D. J. (2014). Dynamic integration of task-relevant visual features in posterior parietal cortex. *Neuron*, *83*(6), 1468–1480.

JASP Team (2017). JASP (Version 0.8.6) [Computer software]. Amsterdam, The Netherlands: University of Amsterdam.

Jeong, S. K., & Xu, Y. (2016). Behaviorally relevant abstract object identity representation in the human parietal cortex. *Journal of Neuroscience*, *36*(5), 1607–1619.

Jigo, M., Gong, M., & Liu, T. (2018). Neural determinants of task performance during feature- based attention in human cortex. *eNeuro*, *5*, ENEURO–0375.

Kamitani, Y., & Tong, F. (2006). Decoding seen and attended motion directions from activity in the human visual cortex. *Current Biology*, *16*(11), 1096–1102.

Kastner, S., & Ungerleider, L. G. (2000). Mechanisms of visual attention in the human cortex. *Annual Review of Neuroscience*, *23*(1), 315–341.

Konen, C. S., & Kastner, S. (2008a). Two hierarchically organized neural systems for object information in human visual cortex. *Nature Neuroscience*, *11*(2), 224–231.

Konen, C. S., & Kastner, S. (2008b). Representation of eye movements and stimulus motion in topographically organized areas of human posterior parietal cortex. *Journal of Neuroscience*, *28*(33), 8361–8375.

Law, C. T., & Gold, J. I. (2008). Neural correlates of perceptual learning in a sensory-motor, but not a sensory, cortical area. *Nature Neuroscience*, *11*(4), 505–513.

Li, S., Ostwald, D., Giese, M., & Kourtzi, Z. (2007). Flexible coding for categorical decisions in the human brain. *Journal of Neuroscience*, *27*(45), 12321–12330.

Liu, T. (2016). Neural representation of object-specific attentional priority. *Neuroimage*, *129*, 15–24.

Liu, T., Hospadaruk, L., Zhu, D. C., & Gardner, J. L. (2011). Feature-specific attentional priority signals in human cortex. *Journal of Neuroscience*, *31*(12), 4484–4495.

Liu, T., & Hou, Y. (2013). A hierarchy of attentional priority signals in human frontoparietal cortex. *Journal of Neuroscience*, *33* (42), 16606–16616.

Mahalanobis, P. C. (1936). On the generalised distance in statistics. *National Institute of Science of India*, *2*, 49–55.

Martinez-Trujillo, J. C., & Treue, S. (2004). Feature-based attention increases the selectivity of population responses in primate visual cortex. *Current Biology*, *14*(9), 744–751.

Miller, E. K., & Cohen, J. D. (2001). An integrative theory of prefrontal cortex function. *Annual Review of Neuroscience*, *24*(1), 167–202.

Navalpakkam, V., & Itti, L. (2006). Top–Down attention selection is fine grained. *Journal of Vision*, *6*(11), 1180–1193.

Prins, N., & Kingdom, F. A. A. (2009). Palamedes: Matlab routines for analyzing psychophysical data. Retrieved from http://www.palamedestoolbox.org

Ptak, R. (2012). The frontoparietal attention network of the human brain: Action, saliency, and a priority map of the environment. *The Neuroscientist*, *18*(5), 502–515.

Riesenhuber, M., & Poggio, T. (1999). Hierarchical models of object recognition in cortex. *Nature Neuroscience*, *2*(11), 1019–1025.

Schluppeck, D., Curtis, C. E., Glimcher, P. W., & Heeger, D. J. (2006). Sustained activity in topographic areas of human posterior parietal cortex during memory-guided saccades. *Journal of Neuroscience*, *26*(19), 5098–5108.

Serences, J. T., & Boynton, G. M. (2007). Feature-based attentional modulations in the absence Of direct visual stimulation. *Neuron*, *55*(2), 301–312.

Sereno, M. I., Dale, A. M., Reppas, J. B., Kwong, K. K., Belliveau, J. W., Brady, T. J., … Tootell, R. B. (1995). Borders of multiple visual areas in humans revealed by functional magnetic resonance imaging. *Science*, *268*(5212), 889–893.

Sereno, M. I., Pitzalis, S., & Martinez, A. (2001). Mapping of contralateral space in retinotopic coordinates by a parietal cortical area in humans. *Science*, *294*(5545), 1350–1354.

Silver, M. A., & Kastner, S. (2009). Topographic maps in human frontal and parietal cortex. *Trends in Cognitive Sciences*, *13* (11), 488–495.

Swaminathan, S. K., & Freedman, D. J. (2012). Preferential encoding of visual categories in parietal cortex compared with prefrontal cortex. *Nature Neuroscience*, *15*(2), 315–320.

Van Essen, D. C. (2005). A population-average, landmark-and surface-based (PALS) atlas of human cerebral cortex. *Neuroimage*, *28*(3), 635–662.

Vaziri-Pashkam, M., & Xu, Y. (2017). Goal-directed visual processing differentially impacts human ventral and dorsal visual representations. *Journal of Neuroscience*, *37*, 8767–8782.

Wagenmakers, E. J. (2007). A practical solution to the pervasive problems of p values. *Psychonomic Bulletion & Review*, *14*(5), 779–804.

Wang, H. X., Merriam, E. P., Freeman, J., & Heeger, D. J. (2014). Motion direction biases and decoding in human visual cortex. *Journal of Neuroscience*, *34*(37), 12601–12615.

Wang, L., Mruczek, R. E., Arcaro, M. J., & Kastner, S. (2015). Probabilistic maps of visual topography in human cortex. *Cerebral Cortex*, *25*(10), 3911–3931.

Warton, D. I. (2008). Penalized normal likelihood and ridge regularization of correlation and covariance matrices. *Journal of American Statsical Association*, *103*(481), 340–349.

Watson, J. D., Myers, R., Frackowiak, R. S., Hajnal, J. V., Woods, R. P., Mazziotta, J. C., … Zeki, S. (1993). Area V5 of the human brain: Evidence from a combined study using positron emission tomography and magnetic resonance imaging. *Cerebral Cortex*, *3*(2), 79–94.

Woolgar, A., Hampshire, A., Thompson, R., & Duncan, J. (2011). Adaptive coding of task-relevant information in human frontoparietal cortex. *Journal of Neuroscience*, *31*(41), 14592–14599.

Zanto, T. P., Rubens, M. T., Bollinger, J., & Gazzaley, A. (2010). Top-down modulation of visual feature processing: The role of the inferior frontal junction. *NeuroImage*, *53*(2), 736–745.

Zhang, X., Mlynaryk, N., Ahmed, S., Japee, S., & Ungerleider, L. G. (2018). The role of inferior frontal junction in controlling the spatially global effect of feature-based attention in human visual areas. *PloS Biology*, *16*(6), e2005399.